Constraining the nuclear pairing gap with pairing vibrations

E. Khan, M. Grasso, and J. Margueron
Institut de Physique Nucléaire, Université Paris-Sud, IN2P3-CNRS, F-91406 Orsay Cedex, France
(Received 26 May 2009; published 27 October 2009)

Pairing interactions with various density dependencies (surface/volume mixing) are constrained with the two-neutron separation energy in the tin isotopic chain. The response associated with pairing vibrations in very neutron-rich nuclei is sensitive to the density dependence of the pairing interaction. Using the same pairing interaction in nuclear matter and in tin nuclei, the optimal range of densities relevant for the pairing channel is also studied.

DOI: 10.1103/PhysRevC.80.044328 PACS number(s): 21.60.Jz, 21.65.Cd, 25.40.Hs, 25.60.Je

I. INTRODUCTION

Studies on pairing effects in both nuclear matter and finite nuclei have known intensified interests in the recent years [1]. There are two main approaches for pairing, depending whether the mean field is based on Gogny finite-range interaction or on Skyrme interaction. In the first approach, a similar functional is used in both the particle-hole channel and the pairing channel, although interactions are not exactly the same due to the density dependence of the pairing interaction: the density-dependent term of the Gogny interaction is omitted in the pairing channel due to its spin-isospin structure not contributing to the $T = 1$, $S = 0$ pairing. In the Skyrme approach, the functionals are meant to differ in the two channels, as witnessed, for instance, by their density dependence The use of a different interaction in the particle-hole channel and in the pairing channel was justified a decade ago [2]; this is, for instance, the case of employing the Skyrme interaction in the particle-hole channel and a zero-range density-dependent interaction in the pairing channel. We shall focus on the Skyrme approach: in this case the pairing density functional is difficult to constrain and it has not been possible to derive an universal pairing interaction during past decades, using, for instance, the odd-even mass staggering on finite nuclei (see, e.g., Refs. [3,4]), although this method has been thoroughly studied [5,6]. This may indicate the need for another approach, using additional constrains: should the pairing density functional be extended and are there additional relevant observables to constrain it? For instance, an extensive survey of odd-even mass staggering showed that a larger strength is required in the proton pairing channel than in the neutron one [7].

Nuclear matter could help in constraining the pairing functional. This requires, however, to bridge nuclei and nuclear matter through local-density approximation (LDA) in the pairing channel: its condition of validity should be more systematically analyzed. It has been recently shown that the two paired neutrons are spatially localized in low-density medium that corresponds to the surface of the nucleus [8]. The same conclusion is drawn by analyzing the dineutron configuration in the excited states [9,10] and also performing calculations in low-density matter in Refs. [11,12], mainly renewing the possibility of linking in some cases the nuclear matter and nuclei in the pairing channel through the LDA.

Concomitantly the pairing functional has been extended to study the condensation of the Cooper pairs (Bose-Einstein condensation and Bardeen-Cooper-Schrieffer crossover) in both symmetric and neutron matter. In nuclear matter the medium polarization increases the pairing gap at low densities in symmetric matter, whereas it reduces the gap in neutron matter, indicating an isospin dependence of the pairing functional [13]. The application to finite nuclei of extended pairing density functional have shown the relevance of the LDA in the pairing channel [14].

The pairing functional studies may thus enter in a new era, renewing the method to design the pairing interaction: (i) using an isospin dependence of the pairing interaction, (ii) using eventually the nuclear matter as an additional constrain for the pairing interaction, (iii) looking for additional observables in nuclei than the odd-even mass staggering to constrain the pairing interaction. Point (i) has been investigated in Refs. [13–15]. Point (ii) requires the validity of the LDA in the pairing channel.

In the case of point (iii) an interesting observable is pairing vibrations, measured through two-particle transfer. It is well known that the transfer cross section crucially depends on the pairing interaction at work in the transferred pair [16,17]. However, in the 1970s and 1980s the form factor of the transition has never been calculated fully microscopically. The first microscopic calculations has been performed only recently [18], allowing for a strong link between the pairing interaction and pairing vibrations. Several calculations followed [9,19], showing the renewed interest for such studies.

It is therefore meaningful to use pairing vibrations as a complementary observable to the masses to constrain the pairing interaction and study the implications to the nuclear matter. One purpose of this work is to evaluate if pairing vibrations could play this role (Sec. III).

The method is to analyze the sensitivity of pairing vibrations to various pairing interactions that provide the same two-neutron separation energy in tin isotopes and evaluate the consequences on the pairing gap in symmetric and neutron matter. On this purpose it is necessary to determine the range of density where pairing gaps are strongly sensitive to the pairing interaction (Sec. II).

II. DENSITY DEPENDENCE OF THE PAIRING OBSERVABLES

After many years of study, there is still no unambiguous universal pairing functional ranging on the whole nuclear chart, and current efforts are aiming in that direction. The problem may be due to the method used to constrain it, namely comparing the pairing gap with odd-even mass differences or evaluating the separation energies along a given isotopic chain. It therefore may be useful to consider a more general context: the evaluation of several pairing interactions constrained by odd-even mass difference, on nuclear matter on the one side and on additional observables on the other side, should shed a renewed light on the problem. To achieve this goal it is first necessary to determine the range of density that is relevant for pairing studies.

A. Method to determine the functional

The method is the following: we first consider surface and various mixed paring interactions. The parameters are determined so as to describe the two neutron separation energy. Then pairing vibrations are used to disentangle between the various pairing interactions (Sec. III). We choose ^{124}Sn and ^{136}Sn nuclei: these are spherical nuclei where pairing vibrations are likely to occur [17]. One is stable and the second has a large neutron excess.

The microscopic calculations for the ground state are based on the Hartree-Fock-Bogoliubov (HFB) model. The Skyrme interaction SLy4 [20] is chosen for the particle-hole channel of the HFB equations. The adopted pairing interaction is the usual zero-range density-dependent interaction

$$V_{\text{pair}} = V_0 \left\{ 1 - \eta \left[\frac{\rho(r)}{\rho_0} \right]^{\alpha} \right\} \delta(\mathbf{r_1} - \mathbf{r_2}), \qquad (1)$$

where η provides the surface/volume character of the interaction. We set $\alpha = 1$ and $\rho_0 = 0.16$ fm^{-3}. The numerical cutoff for the microscopic calculations is given by $E_{\text{max}} = 60$ MeV (in quasiparticle energies) and $j_{\text{max}} = 15/2$. For each value of η, V_0 is chosen to fit the known experimental two-neutron separation energies for even-even $^{114-134}$Sn isotopes. The typical rms value obtained on this observable, compared to the experimental data, is several hundreds of keV. Surface and mixed interactions have been considered in this work and the used values of (η, V_0) are listed in Table I. It should be noted that there is no ideal method to adjust this strength. Using the pairing gap could also be considered. However, only even-even nuclei are calculated, and one cannot directly compare the pairing gap to the experimental odd-even mass difference. Therefore only the trend of the experimental pairing gaps has to be reproduced, as well as their overall magnitude. Using S_{2n} is just an alternative method and we have checked that the corresponding average pairing gaps are of the expected magnitude, typically between 1 and 2 MeV in the Sn isotopes.

TABLE I. Values of η and V_0 of the pairing interaction.

η	V_0 (MeV fm^{-1})
0.35	−285
0.65	−390
1	−670

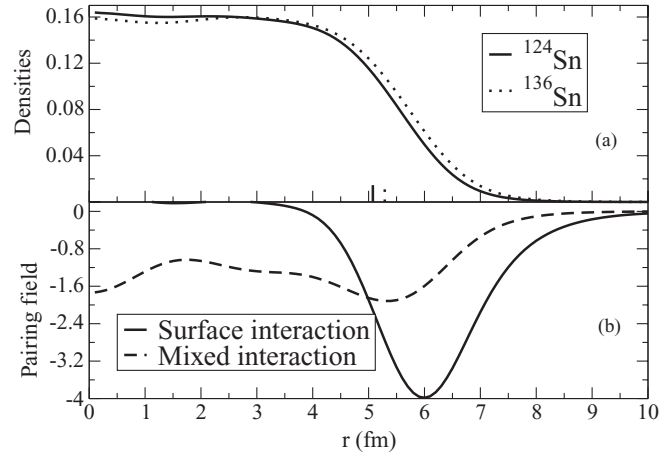

FIG. 1. (a) Matter densities calculated with the HFB model for ^{124}Sn and ^{136}Sn. The vertical lines indicate the radius corresponding the density at which all the pairing interactions converge in uniform matter (see text). (b) Pairing field of ^{124}Sn calculated with a surface $\eta = 1$ (top) and a mixed $\eta = 0.35$ (bottom) pairing interaction.

As an illustration to visualize the features of the calculated pairing effects, we display in Fig. 1 the neutron pairing field for ^{124}Sn corresponding to the surface $\eta = 1$ and the mixed $\eta = 0.35$ interactions.

B. Pairing gap in uniform matter

The relation between the pairing gap in uniform matter at a given density and the pairing field at a given radius in nuclei has been explored in Ref. [14]. It has been found that in the case of mixed interactions, the LDA is in good agreement with the full microscopic HFB calculation (differences less than 15% on the pairing field). This might be related to the extension of the Cooper pair that is getting smaller at the surface of nuclei (about 2 fm) compared to that in the interior (about 5–6 fm) [8]. Close to the surface, pairing properties shall not be very different from that of a uniform piece of matter at the same density. It is then interesting to explore the low-density properties of the different pairing interactions listed in Table I.

Figure 2 displays the pairing gap in uniform matter for various pairing interactions. It is observed that the different interactions leads to very different pairing gap at low density while around saturation density, there is a density ($\rho = 0.11$ fm^{-3}) at which the pairing gap and pairing strength coincide for the three pairing interactions.

From Fig. 2, two conclusions can be drawn: (i) the two-neutron separation energy used to adjust the parameters of the pairing interaction is an observable that provides a strong constraint on the pairing gap localized at the surface of the nuclei: the pairing gap in nuclear matter has been constrained for $\rho = 0.11$ fm^{-3}, which corresponds to $R \simeq 5$ fm in tin nuclei, as shown by the ^{124}Sn densities displayed on Fig. 1; (ii) to better constrain the value of the parameter η, one shall

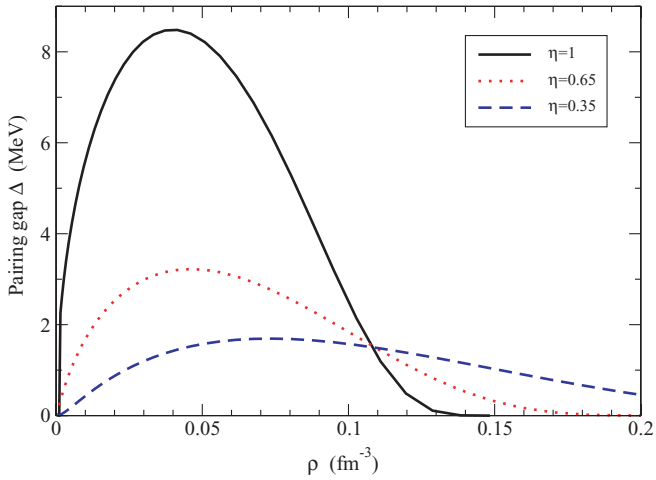

FIG. 2. (Color online) Pairing gap versus the density for uniform matter for different pairing interactions.

find another observable sensitive to the pairing strength at low density (large radius, experimentally easier to probe). Indeed, in the very external part of the nuclei the pairing strength differs significantly from one interaction to another. The pure surface pairing interaction predicts a pairing gap as high as 8 MeV at low density while the various mixed pairing interactions are grouped below 3 MeV (see Fig. 2).

Therefore, one might expect that properties of collective modes sensitive to the external part of the nuclei could be changed by the properties of the pairing interaction at low density. Pair transfer reaction mechanisms like (p, t) or $(\alpha, {}^6\mathrm{He})$ that are very surface peaked shall also help to extract the value of the pairing gap in the external part of nuclei or equivalently at low density.

III. PAIRING VIBRATIONS

As stated above, it may be useful to consider an additional observable than the separation energy to constrain the pairing interaction, namely its density dependence. There are only a few observables that could be relevant to constrain pairing effects. It has been shown that the first 2^+ state in nuclei is sensitive to the pairing interaction [21]: both its position and strength depend of the pairing interaction. However, this is related mainly to the pairing gap value, which is the same observable extracted from odd-even mass difference. It should be noted than none of these two observables (the first 2^+ state and the odd-even mass staggering) can be directly linked to predictions. On the one hand, there is the difficulty to modelize excited states. On the other hand, the difficulty is to describe odd nuclei.

Pairing vibrations may be a more adequate observable. They can be probed, for instance, with two neutrons transfer in nuclei close to shell closure. We refer to Refs. [16,17] for details on pairing vibrations. Basically, these modes correspond to the (collective) filling of subshells, in a transition from an A to $A + 2$ nuclei.

With pairing vibrations, pairing effects are probed in three ways. The first one is the magnitude of the pairing gap Δ (average of the pairing field): a large pairing gap implies strength at larger energies, following the formula $E^2 \simeq (\epsilon - \lambda)^2 + \Delta^2$. This component is also present in the first 2^+ state in the ph response as well as in the odd-even mass staggering. But in the case of the pairing vibrations, there are two additional contributions: first, the transition densities generating the strength are the pairing one, which means that the unperturbed response as well as the perturbed response are sensitive to the impact of the pairing on the wave functions. Finally, the residual interaction, generating the quasiparticle random-phase approximation (QRPA) response, is also sensitive to pairing. Therefore using both the unperturbed and the QRPA response functions, the relative pairing dependence of the wave functions and the residual interaction can be probed.

Pairing vibrations are therefore expected to be very sensitive to the pairing interaction. On the other hand, it may also be difficult to disentangle among the three above-mentioned effects. However, the first one can be evaluated using the energies of the unperturbed response, the second one by studying the pairing transition densities, and the last one by comparing the unperturbed and the QRPA responses. It should be noted that a related study will also be performed in Ref. [22].

A. Method: QRPA in the pp channel

The method is described in Refs. [18,21]. Namely the QRPA equations are solved in coordinate space, using the Green's functions formalism. The variation of the generalized density $\mathcal{R}'$ is expressed in term of three quantities, namely ρ', κ', and $\bar{\kappa}'$, which are written as a column vector:

$$\rho' = \begin{pmatrix} \rho' \\ \kappa' \\ \bar{\kappa}' \end{pmatrix}, \tag{2}$$

where $\rho'_{ij} = \langle 0|c_j^\dagger c_i|'\rangle$ is the variation of the particle density, $\kappa'_{ij} = \langle 0|c_j c_i|'\rangle$ and $\bar{\kappa}'_{ij} = \langle 0|c_j^\dagger c_i^\dagger|'\rangle$ are the fluctuations of the pairing tensor associated to the pairing vibrations, and $|'\rangle$ denotes the change of the ground-state wave function $|0>$ due to the external field. In contrast with the RPA where one needs to know only the change of the ph density (ρ'), the variation of the three quantities (2) have to be calculated in the QRPA. In the three-dimensional space introduced in Eq. (2), the first dimension represents the particle-hole (ph) subspace, the second the particle-particle (pp) one, and the third the hole-hole (hh) one. The response matrix has therefore nine coupled elements in QRPA, compared to one in the RPA formalism.

The variation of the HFB Hamiltonian is given by:

$$H' = \mathbf{V}\rho', \tag{3}$$

where $\mathbf{V}$ is the matrix of the residual interaction expressed in terms of the second derivatives of the HFB energy functional, namely:

$$\mathbf{V}^{\alpha\beta}(\mathbf{r}\sigma, \mathbf{r}'\sigma') = \frac{\partial^2 \mathcal{E}}{\partial\rho_\beta(\mathbf{r}'\sigma')\partial\rho_{\tilde{\alpha}}(\mathbf{r}\sigma)}, \quad \alpha, \beta = 1, 2, 3. \tag{4}$$

In the above equation the notation $\bar{\alpha}$ means that whenever α is 2 or 3 then $\bar{\alpha}$ is 3 or 2.

The QRPA Green's function G can be used for calculating the strength function associated with the two-particle transfer from the ground state of a nucleus with A nucleons to the excited states of a nucleus with $A+2$ nucleons. This strength function is:

$$S(\omega) = -\frac{1}{\pi}\mathrm{Im}\int F^*(\mathbf{r})\mathbf{G}^{22}(\mathbf{r},\mathbf{r}';\omega)F(\mathbf{r}')\,d\mathbf{r}\,d\mathbf{r}', \qquad (5)$$

where $\mathbf{G^{22}}$ denotes the (pp,pp) component of the Green's function and F is the external perturbating field associated with the addition of two particles.

The residual interaction in the pp,pp channel is the pairing interaction. However, when solving the Bethe-Salpeter (BS) equation, the Green's functions G and the residual interaction are 3×3 matrices, with ph, pp, and hh dimensions [Eq. (4)]. Solving the BS equation couples these dimensions. Therefore, there is, for instance, an effect of the ph,pp component of the residual interaction on the pp,pp channel.

In the QRPA calculations the full HFB quasiparticle spectrum up to 60 MeV is included. These states are used to construct the unperturbed Green's function $\mathbf{G_0}$. The residual interaction is derived from the two-body force used in HFB according to Eq. (4). The contribution given by the velocity-dependent terms of the Skyrme force to the residual interaction is calculated in the Landau-Migdal approximation, which is shown to be accurate [23]. The strength function for the two-neutron transfer is calculated using Eq. (5). The unperturbed Green's function is calculated with an averaging interval equal to 0.15 MeV. All details can be found in Ref. [18].

The response function is calculated for the pp channel. All the calculations are performed in a box of size 22.5 fm. It should be noted that exact continuum treatment is heavy, especially for nuclei such as Sn isotopes. Moreover the aim is not to study the impact of the continuum treatment (see Ref. [18] for such a study). Finally, the Sn isotopes under study are far from the drip line, and continuum effects are expected to play a negligible role.

B. Unperturbed response results

The HFB solutions are used in the QRPA scheme to analyze self-consistently the excitation modes associated to the pair transfer reactions. Because we study here two-neutron transfers, we focus on the neutron HFB quasiparticle states that are used to construct the elementary configurations of the excited modes. We work with positive-energy quasiparticle states. Once calculated the quasiparticle spectrum, it is possible to deduce some properties of the unperturbed response function.

The quasiparticle states with energy less than 6 MeV and an occupation probability $\leqslant 80\%$ are presented in Tables II and III for ^{124}Sn and ^{136}Sn, respectively. Let us discuss the two cases $\eta = 0.35$ and $\eta = 1$ (for $\eta = 0.65$, results are similar to those obtained with $\eta = 0.35$). For ^{124}Sn, in the case of a mixed pairing interaction, $\eta = 0.35$, all the quasiparticle states with energy lower than 5 MeV are totally occupied with the exception of a $h_{11/2}$ state at 1.5 MeV that is 42% occupied. This is the only low-energy state that can contribute to some extent to the excitation mode. The states that are completely empty and can thus contribute more to the excitation are located at higher energies. The first is an $f_{7/2}$ state at 5.8 MeV. The others have larger energies (at least 1 MeV more). One can thus expect that the unperturbed response profile starts with a peak at twice 5.8 MeV, i.e., at ~11.6 MeV (with some small contribution at 3 MeV). In the case of a surface interaction, $\eta = 1$, again, all the states between 0 and 5 MeV are occupied

TABLE II. Neutron quasiparticle states with $E \leqslant 6$ MeV and occupation less than 80%. The nucleus is ^{124}Sn.

η	State	E (MeV)	occ
0.35	$h11/2$	1.5	0.42
	$f7/2$	5.8	0.01
0.65	$h11/2$	1.7	0.42
	$f7/2$	5.7	0.01
1	$h11/2$	2.2	0.42
	$p3/2$	5.4	0.003
	$f7/2$	5.5	0.02
	$p1/2$	5.6	0.002
	$s1/2$	5.7	0.002

TABLE III. Same as in Table II but for ^{136}Sn.

η	State	E (MeV)	occ
0.35	$f7/2$	0.8	0.45
	$p3/2$	1.9	0.01
	$p1/2$	2.4	0.006
	$f5/2$	2.9	0.01
	$s1/2$	3.3	0.0005
	$d5/2$	4.0	0.0002
	$d3/2$	4.1	0.0005
	$g9/2$	5.6	0.0001
	$g7/2$	5.6	0.0001
0.65	$f7/2$	0.9	0.43
	$p3/2$	1.9	0.02
	$p1/2$	2.4	0.008
	$f5/2$	2.9	0.02
	$s1/2$	3.2	0.0004
	$d5/2$	3.9	0.0001
	$d3/2$	3.9	0.0003
	$g9/2$	5.4	0.0001
	$g7/2$	5.5	0.00003
1	$f7/2$	1.6	0.32
	$p3/2$	1.7	0.02
	$p1/2$	1.9	0.01
	$s1/2$	1.9	0.0004
	$d5/2$	2.6	0.0003
	$d3/2$	2.6	0.0002
	$f5/2$	3.0	0.01
	$g9/2$	4.1	0.0002
	$g7/2$	4.1	0.0001

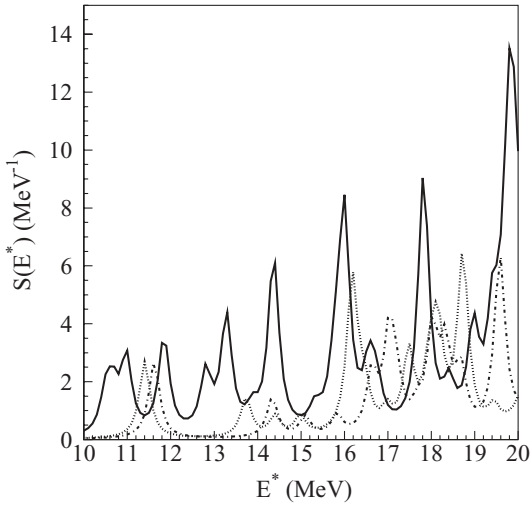

FIG. 3. Unperturbed response function for ^{124}Sn in the two neutrons 0^+ addition mode. The pure surface mode is shown with the solid line, the $\eta = 0.65$ mode is shown with the dotted line, and the $\eta = 0.35$ mode isshown with the dashed-dotted line.

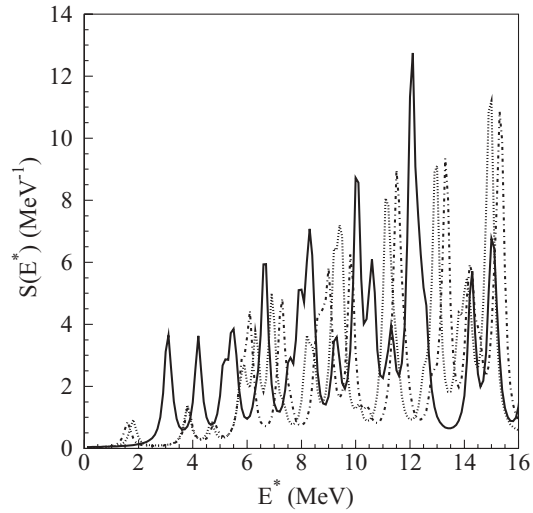

FIG. 4. Unperturbed response function for ^{136}Sn in the two neutrons 0^+ addition mode. The pure surface mode is shown with the solid line, the $\eta = 0.65$ mode is shown with the dotted line, and the $\eta = 0.35$ mode shown with the dashed-dotted line.

with the exception of a $h_{11/2}$ state at 2.2 MeV (42% of occupation). This time there are several unoccupied states just above 5 MeV, the lowest energy being at 5.4 MeV ($p_{3/2}$ state). Hence, the unperturbed response is expected to have some structure starting from ∼10.8 MeV with a small contribution at ∼4.4 MeV.

For the nucleus ^{136}Sn the situation is different: there are several low-lying unoccupied states. For $\eta = 0.35$ the lowest energy for a completely unoccupied state is 1.9 MeV ($p_{3/2}$ state). At 0.8 MeV one also finds a $f_{7/2}$ state with 45% of occupation. In the case $\eta = 1$ the lowest energy for a totally unoccupied state is 1.7 MeV ($p_{3/2}$ state) and a $f_{7/2}$ state is found at 1.6 MeV with 32% of occupation. The unperturbed response is expected to start at ∼3.8 and 3.2 MeV for $\eta = 0.35$ and 1, respectively. In the former case a small contribution at ∼1.6 MeV is also expected.

To disentangle the various pairing effects, the unperturbed response in the two neutrons addition mode is first shown in Fig. 3 for ^{124}Sn. The unperturbed response is built on the HFB single quasiparticle (QP) spectrum for the three pairing interactions. It should be noted that the spectrum is shown above 10 MeV, because there is only the $h_{11/2}$ subshell that can welcome two neutrons to make a low-energy state: all the other configurations belong to the next major shell (see Table II), explaining this high-energy feature of the spectrum, as stated above. For all the mixed pairing interaction, the unperturbed spectrum is similar, showing that both the single quasiparticle energy and wave functions are close to each other in that case. However, in the case of the pure surface pairing, the spectrum is changed. The energies are shifted to lower values, and the overall strength is increased. The lower energy shift can be understood by more single-quasiparticle states located at low energy. This can be explained by a lower pairing gap and a different energy spectrum found in the HFB self-consistent procedure. The larger magnitude comes from the wave functions and will be studied with the QRPA response. It can already be stated that the QRPA response will also have more strength at lower energy, due to this peculiar feature of the unperturbed spectrum for the pure surface pairing force.

Figure 4 shows the unperturbed response for the two neutron addition mode in ^{136}Sn. In this case, at the beginning of an open neutron shell several low-energy configurations can welcome the two neutrons (see Table III). As in the case of ^{124}Sn, the response exhibits larger strength at low energy in the specific case of the pure surface pairing interaction compared to others pairing interaction. This is related to the pairing field profile as shown on Fig. 1. It should be noted that to clearly see the effect due to the surface pairing, not only the first 0^+ state but also the energy area of a few MeV above should be explored because the results are different from 0 to 4 MeV on Fig. 4.

C. Perturbed response results

Figure 5 shows the QRPA response for ^{124}Sn, with a pure surface and the two mixed interactions. As expected the residual interaction plays a similar role in all the cases, gathering strength and shifting it to lower energy. In the case of ^{124}Sn, a peak around 9 MeV is the strongest for the surface pairing interaction, to be compared with the one around 10 MeV for the other interactions. Hence it is expected that the pairing vibration transition strength should be larger in the case of a pure surface force. However, it is known that it is difficult to accurately describe the magnitude of these transitions, especially for absolute cross-section calculations [24]: one-step or sequential two-step process, triton wave function, and zero-range or finite-range distorted-wave Born approximation (DWBA) have to be considered. The main elements of such a calculation are the optical potentials in both the entrance and the exit channel: they can be either phenomenological such as the Becchetti and Greenlees optical

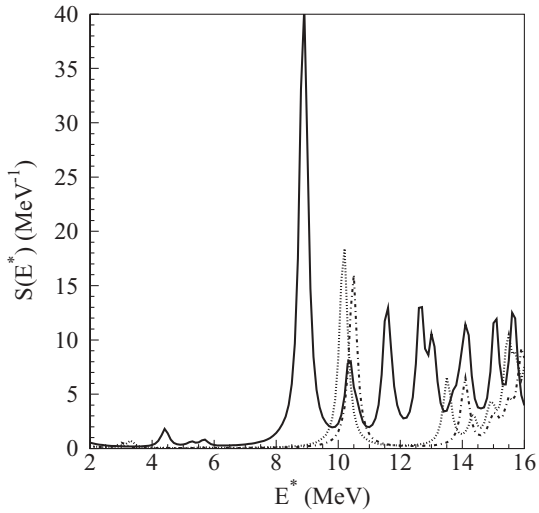

FIG. 5. QRPA response function for ^{124}Sn in the two neutrons 0^+ addition mode. The pure surface mode is shown with the solid line, the $\eta = 0.65$ mode is shown with the dotted line, and the $\eta = 0.35$ mode is shown with the dashed-dotted line.

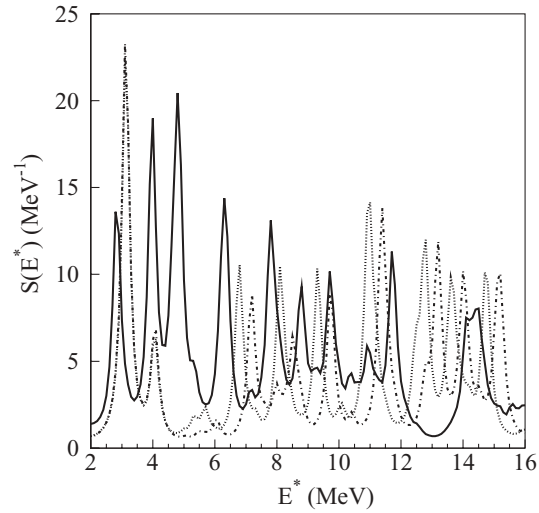

FIG. 7. QRPA response function for ^{136}Sn in the two neutrons 0^+ addition mode. The pure surface mode is shown with the solid line, the $\eta = 0.65$ mode is shown with the dotted line, and the $\eta = 0.35$ mode is shown with the dashed-dotted lines.

potential [25] or microscopic by using a double folding approach. The other relevant element is the form factor related to the reaction, which includes the information on nuclear structure: it is expected that the relative magnitude of the angular distributions of two 0^+ states remains mainly sensitive to the form factor, related itself to the pairing transition density (Eq. (41) of Ref. [17]). It should be noted that in the case of zero-range DWBA, the pairing transition density directly provides the form factor.

The pairing transition density is defined as:

$$\kappa^{\nu}(\mathbf{r}, \sigma) = \langle 0 | c\ (\mathbf{r},\ \bar{\sigma})\ c(\mathbf{r}, \sigma)\ | \nu \rangle, \tag{6}$$

where $c^{\dagger}(\mathbf{r}, \bar{\sigma}) = -2\sigma c^{\dagger}(\mathbf{r}, -\sigma)$ is its time-reversed counterpart.

It allows us to calculate the form factor in the zero-range DWBA approximation. The pairing transition densities of Fig. 6 show, in the case of ^{124}Sn, a difference, going from surface to other modes: the transition density decreases at the surface. However, the difference is not dramatic and may be over-ruled by the experimental uncertainties. The larger strength of the 9 MeV peak in the pure surface pairing interaction is due to a larger transition density at the surface.

For the ^{136}Sn neutron-rich nucleus, the low-energy spectrum displayed on Fig. 7 is dramatically changed from using surface to other interactions on a several-MeV area. A three-peak structure appears in the surface case compared to the two peaks structure of the other cases. The integrated strength is also larger in the surface case.

Figures 8 and 9 show the corresponding transition densities. They exhibit very different shapes, comparing results with the pure surface pairing interaction and the mixed pairing interaction. Hence ^{136}Sn is a good test case to probe the pairing interaction through pairing vibrations. For instance, in the case of the most intense peak, the central part is dominant in the transition density for the mixed case, whereas the surface part of the transition density dominates in the pure surface

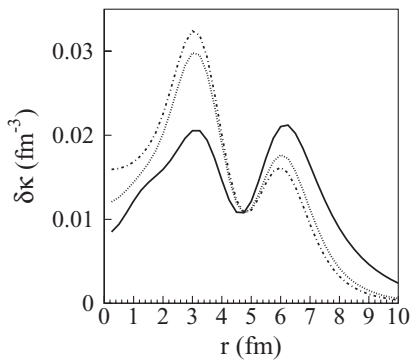

FIG. 6. Neutron transition density in the two neutrons addition mode for ^{124}Sn for the first peak located at 9–10 MeV. The pure surface mode is shown with the solid line, the $\eta = 0.65$ mode is shown with the dotted line, and the $\eta = 0.35$ mode is shown with the dashed-dotted line.

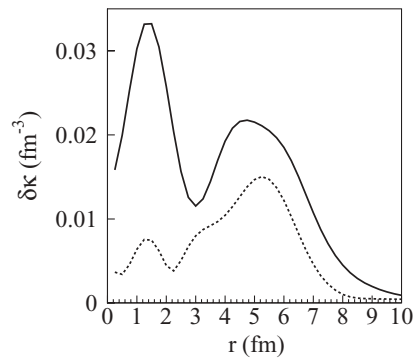

FIG. 8. Neutron transition density in the two neutrons addition mode for ^{136}Sn for the first two peaks of the strength in the case of the mixed $\eta = 0.65$ interaction.

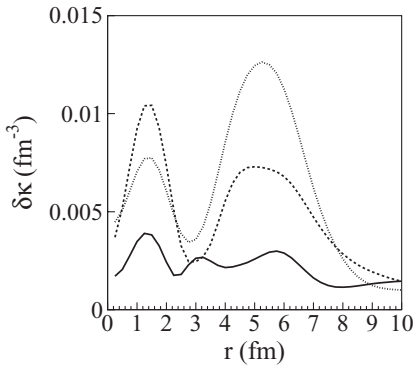

FIG. 9. Neutron transition density in the two-neutron addition mode for ^{136}Sn for the first three peaks of the strength in the case of the pure surface interaction.

interaction. Hence a measurement of the angular distributions associated with the pairing vibration strength in very neutron rich-nuclei such as ^{136}Sn seems more decisive to disentangle between the pairing interactions than with ^{124}Sn. This may be due to the larger neutron skin in ^{136}Sn, consisting of low-density neutron-rich matter.

It has been shown in a previous work how the pairing transition densities allows us to calculate the two neutron form factor to predict angular distributions for pairing vibrations [18]. Work along these lines should be undertaken to bring additional constrains on the pairing interaction. Recently dynamical approaches related to pairing have been developed, such as the time-dependent HFB model [19]. They can also be tested using pairing vibrations, through their calculated transitions densities, in a similar way than the present method.

IV. CONCLUSIONS

The impact of various pairing interactions on pairing vibrations predictions has been analyzed for the first time using an HFB + QRPA approach. They should provide a good sensitivity from a pure surface interaction compared to mixed interactions, especially in the case of very neutron-rich nuclei such as ^{136}Sn. Moreover nuclear matter gap calculations show that the low-density range is sensitive to the surface/volume character of the pairing interaction. In the case of exotic nuclei, pairing vibrations are also found more sensitive to the surface/volume type of the pairing interaction than in the case of stable nuclei. This may be due to the larger extension of the neutron density in very neutron-rich nuclei.

The same study using an isospin-dependent pairing interaction will be undertaken. The hope is to come one step closer to a more global pairing interaction, using odd-even mass staggering, pairing vibrations, and nuclear matter as constraints. Experimentally, the pairing transition densities can be tested through the form factor used to calculate the two-neutron-transfer cross section. This implies to use a adequate reaction model. Work along these lines will be undertaken in an near future.

ACKNOWLEDGMENTS

The authors thank D. Beaumel, M. Matsuo, and A. Vitturi for fruitful discussions.

[1] D. J. Dean and M. Hjorth-Jensen, Rev. Mod. Phys. **75**, 607 (2003).
[2] E. Garrido, P. Sarriguren, E. Moya de Guerra, and P. Schuck, Phys. Rev. C **60**, 064312 (1999).
[3] J. Dobaczewski, H. Flocard, and J. Treiner, Nucl. Phys. **A422**, 103 (1984).
[4] S. Goriely, M. Samyn, and J. M. Pearson, Phys. Rev. C **75**, 064312 (2007).
[5] J. Dobaczewski, P. Magierski, W. Nazarewicz, W. Satula, and Z. Szymanski, Phys. Rev. C **63**, 024308 (2001).
[6] T. Duguet, P. Bonche, P.-H. Heenen, and J. Meyer, Phys. Rev. C **65**, 014310 (2001); **65**, 014311 (2001).
[7] G. F. Bertsch, C. A. Bertulani, W. Nazarewicz, N. Schunck, and M. V. Stoitsov, Phys. Rev. C **79**, 034306 (2009).
[8] N. Pillet, N. Sandulescu, and P. Schuck, Phys. Rev. C **76**, 024310 (2007).
[9] M. Matsuo, K. Mizuyama, and Y. Serizawa, Phys. Rev. C **71**, 064326 (2005).
[10] K. Hagino and H. Sagawa, Phys. Rev. C **76**, 047302 (2007).
[11] M. Matsuo, Phys. Rev. C **73**, 044309 (2006).
[12] K. Hagino, H. Sagawa, J. Carbonell, and P. Schuck, Phys. Rev. Lett. **99**, 022506 (2007).
[13] J. Margueron, H. Sagawa, and K. Hagino, Phys. Rev. C **76**, 064316 (2007).
[14] J. Margueron, H. Sagawa, and K. Hagino, Phys. Rev. C **77**, 054309 (2008).
[15] M. Yamagami, Y. R. Shimizu, and T. Nakatsukasa, arXiv:0812.3197 (2008).
[16] R. A. Broglia, O. Hansen, and C. Riedel, Adv. Nucl. Phys. **6**, 287 (1973).
[17] W. von Oertzen and A. Vitturi, Rep. Prog. Phys. **64**, 1247 (2001).
[18] E. Khan, N. Sandulescu, N. V. Giai, and M. Grasso, Phys. Rev. C **69**, 014314 (2004).
[19] B. Avez, C. Simenel, and Ph. Chomaz, Phys. Rev. C **78**, 044318 (2008).
[20] E. Chabanat, P. Bonche, P. Haensel, J. Meyer, and R. Schaeffer, Nucl. Phys. **A635**, 231 (1998).
[21] E. Khan, N. Sandulescu, M. Grasso, and N. V. Giai, Phys. Rev. C **66**, 024309 (2002).
[22] M. Matsuo, Proceedings of COMEX 3 Conference, Mackinac Island, USA (2009).
[23] K. Mizuyama, M. Matsuo, and Y. Serizawa, Phys. Rev. C **79**, 024313 (2009).
[24] M. Igarashi, K. Kubo, and K. Yagi, Phys. Rep. **199**, 1 (1991).
[25] F. D. Becchetti and G. W. Greenlees, Phys. Rev. **182**, 1190 (1969).